ISSN (ONLINE): 2454-9762
ISSN (PRINT): 2454-9762
Available online at www.ijarmate.com

International Journal of Advanced Research in Management, Architecture, Technology and Engineering (IJARMATE)
Vol. 3, Special Issue10, March 2017

Application of CCM zeta micro inverter for solar photovoltaic AC module

S.Selgin[1], Mrs.Smitha[2]
[1]PG student, Power Electronics and Drives, Ponjesly College of Engineering
[2]Assistant Professor, Department of EEE, Ponjesly College of Engineering
[1]selginsel@gmail.com

Abstract-Zeta Micro inverter mounted on each photovoltaic panel, micro inverter is gaining popularity due to increased energy harvest. Single stage zeta micro inverter is available for PV applications. The proposed topology is based on zeta converter with high frequency transformer isolation and single low side switch on the primary side of transformer. The most distinctive feature of the proposed inverter is its ability to work in continuous conduction mode over a wide load range, which results in high efficiency, reduced current stress, and components rating, reducing number of power conversion stages, and scalability. All the secondary switches operate at line frequency, thus reducing switching losses significantly. Micro inverters are attached at the back of a PV panel and directly generate AC with MPPT. The proposed system of micro inverter including steady-state analysis and design has been involved. A 220W micro inverter was designed, developed, and tested in the laboratory. Experimental results are demonstrated to verify the CCM operation of the inverter and its performance over a wide load range.

Keywords—Photovoltaic (PV), AC module, Zeta, Microinverter, Continuous Conduction Mode (CCM).

I. INTRODUCTION

Among various renewable energy sources, solar is the most abundant form of energy. Series connected PV panels with a single large inverter (string inverter) can be used to feed power into the grid with a common Maximum Power Point Tracking (MPPT). However, this is an inefficient way of harvesting energy because individual MPPT of solar panels is not done. A panel mismatch, shading or formation of debris will reduce the energy harvest significantly.Various inverter topologies are presented, compared, and evaluated against demands, lifetime, component ratings, and cost. Finally, some of the topologies are pointed out as the best candidates for either single PV module or multiple PV module applications [9].A review of the appropriate storage-system technology used for the integration of intermittent renewable energy sources is also introduced.Theeffects of power-system operation, especially where the intermittent energy source constitutes a significant part of the total system capacity[1].

A full bridge connected to a high-frequency transformer and a full-bridge rectifier amplifies the voltage of the PV panel to approximately 475 V. This stage is controlled by using a phase-shift pulsewidth-modulation controller that permits zero-voltage switching, thereby minimizing losses.The performance of PV modules is easy to be affected by partial shadows and mismatch of their electrical parameters. Consequently, the conventional power configurations are difficult to obtain higher energy efficiency and reliability. Some improved power configurations of BIPV system have been presented to solve these problems[13]. The transformer leakage energy is handled by the decoupling circuit itself so there is no need for additional dissipative circuits, which leads to reduced power losses and improved efficiency[6].

II SINGLE STAGE CCM ZETA MICRO INVERTER

Modeling of zeta dc/dc converter and parameter selection is important to eliminate RHP zero. It is concluded that zeta converter can achieve higher bandwidth, and good closed loop stability. A DCM mode zeta converter based inverter. The inverter power rating was limited to 80W. Low switching frequency (20 kHz) operation resulted into a larger filter and transformer. A single stage CCM zeta micro-inverter is proposed as shown in Fig 1, with a single primary switch and four secondary switches working as LFI.

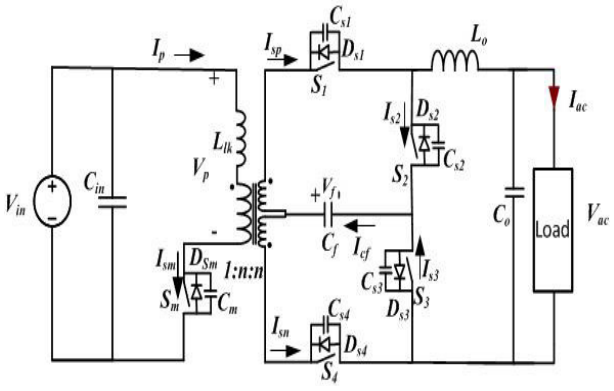

Fig 1: Zeta Microinverter

The steady-state operation of proposed microinverter. To simplify analysis, the following assumptions are made: (i) All semiconductor devices are ideal and lossless (ii) input

ISSN (ONLINE): 2454-9762
ISSN (PRINT): 2454-9762
Available online at www.ijarmate.com

International Journal of Advanced Research in Management, Architecture, Technology and Engineering (IJARMATE)
Vol. 3, Special Issue10, March 2017

voltage ripple is negligible. Operation of zeta microinverter is explained for the positive half cycle of load current at switching frequency. The main switch $S_m$is modulated at high frequency with a variable duty cycle to generate rectified ac output and secondary switches $S_1 - S_4$ are operated at line frequency to produce ac output at line frequency. On the secondary side, during positive half cycle of load current switches S_1, S_3 are gated to conduct and during negative half cycle of load current, switches S_2, S_4 are gated to conduct. Steady-state operation of the proposed microinverter in DCM and CCM mode of operation is analyzed.

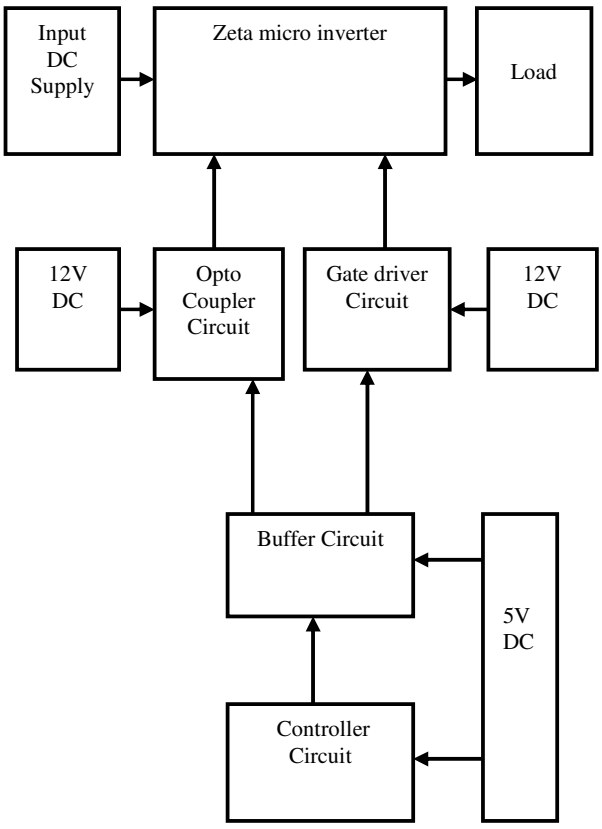

Fig 2: Block Diagram of Single Stage CCM Zeta Micro Inverter

From the block diagram (Fig 2) the solar panel the power is sent to the isolated zeta converter. The converter is used to convert the power from DC to AC. The control circuit consists of Opto coupler, Gate driver and Buffer. The programmable interface controller is act as a microcontroller. The output of the zeta converter is given to the single phase inverter. In order to fed to the grid it is inverted and the output of the inverter is filtered by using LC filter. So the harmonics of the inverter will be reduced. The AC output is given to the grid. The efficiency of the system will be improved because of the micro inverter operating at continuous conduction mode. So the switching losses will be reduced.

III DCM MODE OF OPERATION

A. Interval 1 ($t_{d0} < t < t_{d1}$) (Fig 3)

At $t = t_{d0}$, the main switch S_m is tuned-on. Secondary switches S_1, S_3 are conducting for the entire positive half cycle of load current. Diode D_{s2} is reverse biased as shown in Fig 3 Primary current $I_p$increases linearly starting from zero as shown in Fig 4 Primary current $I_p$and magnetizing inductor current I_{lm}can be given as

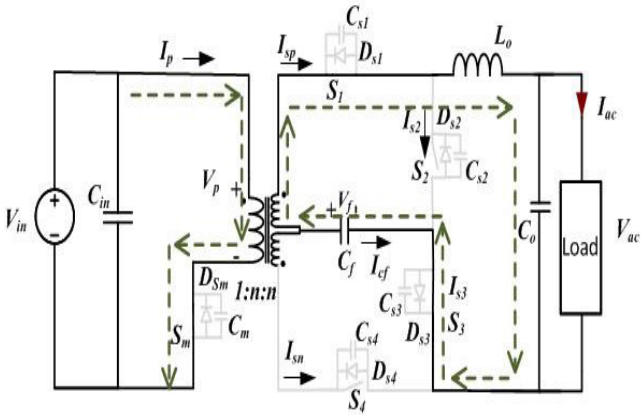

Fig 3:Interval 1 ($t_{d0} < t < t_{d1}$)

$$i_p(t) = \left(\frac{V_{in}}{L_m} + \frac{n^2 V_o}{L_o}\right)(t - t_{d0}) \quad (1)$$

$$i_m(t) = I_{lm}(t_{d0}) + \frac{V_{in}}{L_m}(t - t_{d0}) \quad (2)$$

In this interval, secondary switch current $i_{s2} = 0$ and secondary side currents i_{sp}, $i_{Lo}$and $i_{cf}$are similar due to series connection as shown in Fig 3 and the values is derived as

$$i_{sp}(t) = \frac{i_p(t) - i_{lm}(t)}{n} = i_{Lo}(t) = -i_{cf}(t) \quad (3)$$

Flying capacitor $c_f$is discharging, and at the end of this interval, its voltage falls below the minimum value, V_{cfmin}

ISSN (ONLINE): 2454-9762
ISSN (PRINT): 2454-9762
Available online at www.ijarmate.com

International Journal of Advanced Research in Management, Architecture, Technology and Engineering (IJARMATE)
Vol. 3, Special Issue10, March 2017

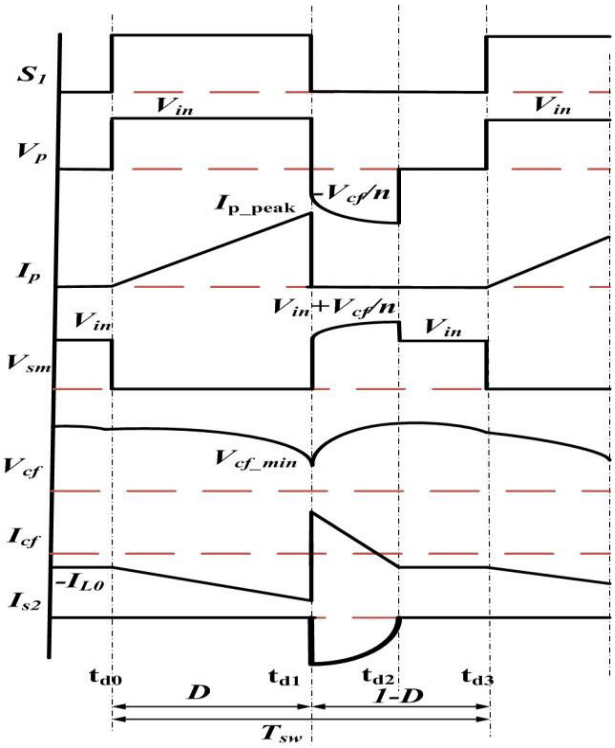

Fig 4: Steady-state operating waveforms of the for proposed inverter in DCM mode of operation

At the end of this interval, primary current i_p reaches maximum value denoted by i_{p_peak} given by (eqn. 4). Duration of this interval is equal to $DT_S(t_{d1} = DT_S)$ where, D is the duty cycle, T_S is the time period of main switch S_m.

$$I_p(t_{d1}) = I_{p\_peak} = \left(\frac{V_{in}}{L_m} + \frac{n^2 V_i}{L_o}\right)(DT_S) \quad (4)$$

$$I_{Lo}(t_{d1}) = I_{Lo\_peak} = \frac{I_{p\_peak} - I_{Lm}(t=t_{d1})}{n} (5)$$

B. Interval 2 $(t_{d1} < t < t_{d2})$ (Fig 5)

At t = t_{d1}, the main switch S_m is turned-off and secondary side diode D_{s2} goes into conduction. At the start of this interval, the diode current is equal to peak primary current I_{p_peak} referred to secondary given by

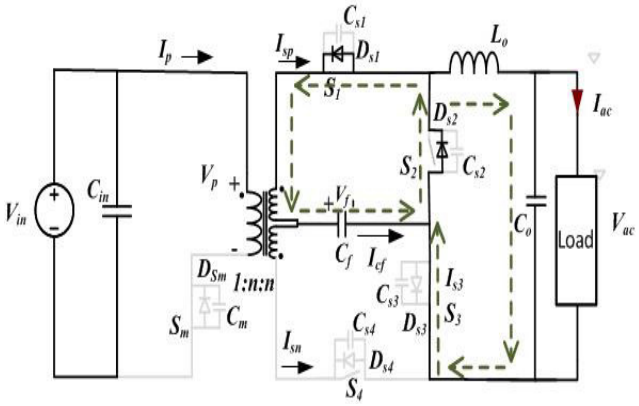

Fig 5: Interval 2 $(t_{d1} < t < t_{d2})$

$$I_{ds2}(t_{d1}) = -I_{s2}(t_{d1}) = \frac{I_{p\_peak}}{n} \quad (6)$$

$$I_{s2}(t_{d1}) = -\frac{I_{p\_peak}}{n} = -\frac{\left(\frac{V_{in}}{L_m} + \frac{n^2 V_i}{L_o}\right)(DT_S)}{n} \quad (7)$$

The magnetizing inductance L_M starts charging the flying capacitor from initial value of V_{cf_min}. Switch current i_{s2} and output inductor current i_{Lo} are given as

$$i_{s2}(t_{d1}) = -\frac{I_{p\_peak}}{n} + \frac{V_o}{L_o}(t - t_{d1}) + \frac{V_{cf}(t)}{n^2 L_m}(t - t_{d1}) \quad (8)$$

$$V_{cf}(t) = V_{cf\_min} + \frac{1}{C_f}\int i_{cf}\, dt \quad (9)$$

$$i_{Lo}(t) = I_{Lo\_peak} - \frac{V_o}{L_o}(t - t_{d1}) \quad (10)$$

It should be noted from (eqn. 9) that with increase in value of flying capacitor, voltage ripple will reduce. Average voltage across the output capacitor and the flying capacitor is equal for given switching cycle $(\ll V_{cf} \gg = \ll V_o \gg)$. Thus, for higher values of flying capacitance, V_{cf} is approximately equal to the output voltage V_o and is constant for a given switching cycle. So, the switch current i_{s2} can be approximated to

$$i_{s2}(t) = -\frac{I_{p\_peak}}{n} + \frac{V_o}{L_o}(t - t_{d1}) + \frac{V_o}{n^2 L_m}(t - t_{d1}) \quad (11)$$

However, for a practical design with higher flying capacitance value, corresponding increase in series resistance of capacitor will increase conduction losses. Although, conduction losses in the diode D_{s2} will reduce with increasing capacitance value. Thus, an optimum value of the flying capacitor should be chosen to limit overall losses. This interval ends when the

ISSN (ONLINE): 2454-9762
ISSN (PRINT): 2454-9762
Available online at www.ijarmate.com

International Journal of Advanced Research in Management, Architecture, Technology and Engineering (IJARMATE)
Vol. 3, Special Issue10, March 2017

switch current i_{s2} becomes zero. This interval can be obtained by my making i_{s2} = 0, and substituting $t = t_{d2}$ and is given by

$$t_{d2} = \frac{\frac{I_{p\_peak}}{n} + \left(\frac{V_o}{L_o} + \frac{V_o}{n^2 L_m}\right)(DT_s)}{\left(\frac{V_o}{L_o} + \frac{V_o}{n^2 L_m}\right)} \quad (12)$$

At the end of this interval, inductor current i_{Lo} is given by

$$i_{Lo}(t_{d2}) = I_{Lo\_peak} - \frac{V_o}{L_o}(t_{d2} - DT_s) \quad (13)$$

C. Interval 3 ($t_{d2} < t < t_{d3}$) (Fig. 3.7)

This interval starts when the secondary diode current i_{s2} becomes zero and extends until the primary switch is turned-on at $t = t_{d3}$. This interval is seen only if inverter goes into DCM and equivalent circuit for this time interval is shown in Fig 6. A voltage $(V_{cf} - V_o)$ appears across the output inductor and its current expression is

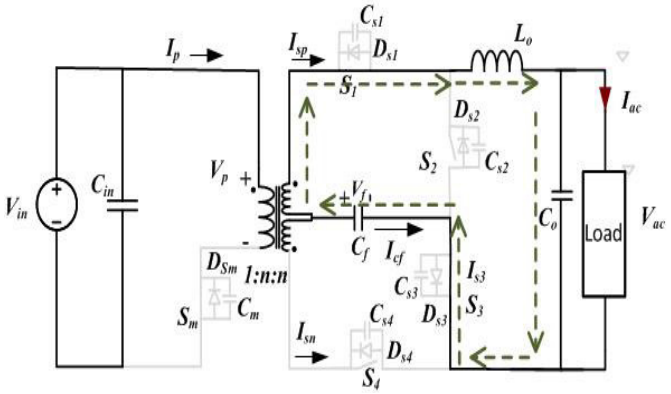

Fig 6:Interval 3 ($t_{d2} < t < t_{d3}$)

$$i_{Lo}(t) = I_{Lo}(t_{d2}) + \frac{V_{cf} - V_o}{L_o}(t - t_{d2}) \quad (14)$$

The second term in (eqn.14) is very small which makes inductor current approximately dc. The same current flows through the magnetizing inductance but negative. At the end of this interval, the current i_{Lo} and i_{lm} are given by

$$i_{Lo}(T_s) = I_{Lo}(t_{d2}) + \frac{V_{cf} - V_o}{L_o}(T_s - t_{d2}) \quad (15)$$

$$I_{lm}(T_s) = I_{lm}(t_{d0}) = -nI_{Lo}(T_s) \quad (16)$$

The inverter operation is repeated at switching frequency with a variable duty cycle *D* to generate a rectified sine output. Once the reference load current is negative, switches S_1 and S_3 are tuned-off, and the switches S_2 and S_4 are turned-on.

III CCM MODE OF OPERATION

A. Interval 1 ($t_{c0} < t < t_{c1}$) (Fig 3)

At $t = t_{c0}$, the main switch S_m is tuned-on and secondary switches S_1 and S_3 are conducting throughout the positive half cycle. Equivalent circuit of the proposed zeta inverter for the current interval is shown in Fig 3 Fig 4 shows the steady state operating waveforms when operated in CCM. This interval is common to both DCM and CCM but prior to this interval the voltage across the primary of the transformer is non-zero, thus the current in the primary starts from a minimum value. In this interval input voltage, V_{in} is applied across the magnetizing inductance L_m of the transformer. Diode D_{s2} is reverse biased, thus the secondary switch current i_{s2} = 0 in this interval. Mathematical equations for the various current waveforms are

$$i_p(t) = I_p(t_{c0}) + \left(\frac{V_{in}}{L_m} + \frac{n^2 V_{in}}{L_o}\right)(t - t_{c0}) \quad (17)$$

$$i_{lm} = I_{lm}(t_{c0}) + \left(\frac{V_{in}}{L_m}\right)(t - t_{c0}) \quad (18)$$

$$i_{s1}(t) = \frac{i_p(t) - i_{lm}(t)}{n} = i_{Lo}(t) = i_{cf}(t) \quad (19)$$

At the end of this interval, flying capacitor is discharged to V_{cf-min}, currents I_p, I_{Lm} and I_{Lo} reach their peak values which can be represented by I_{p-peak}, $I_{Lm-peak}$ and $I_{Lo-peak}$, respectively and are given by

$$I_p(t_{c1}) = I_{p\text{-}peak} = I_p(t_{c0}) + \left(\frac{V_{in}}{L_m} + \frac{n^2 V_{in}}{L_o}\right)(DT_s) \quad (20)$$

$$I_{Lm}(t_{c1}) = I_{Lm-peak} = I_{Lm}(t_{c0}) + \left(\frac{V_{in}}{L_m}\right)(DT_s) \quad (21)$$

$$I_{Lo}(t_{c1}) = I_{Lo-peak} = \frac{I_{p-peak} - I_{Lm-peak}}{n} \quad (22)$$

This interval with duration DT_s ends when the main switch S_m is tuned-off.

B . Interval 2 ($t_{c1} < t < t_{c2}$) (Fig 5)

At $t = t_{c1}$ the main switch S_m is turned-off and secondary side diode D_{s2} goes into conduction as shown in Fig 5. At the start of this interval, the diode current is equal to peak primary current I_{p-peak} referred to secondary, which can be given as

$$I_{ds2}(t_{c1}) = -I_{s2}(t_{c1}) = \frac{I_{p-peak}}{n} \quad (23)$$

ISSN (ONLINE): 2454-9762
ISSN (PRINT): 2454-9762
Available online at www.ijarmate.com

International Journal of Advanced Research in Management, Architecture, Technology and Engineering (IJARMATE)
Vol. 3, Special Issue10, March 2017

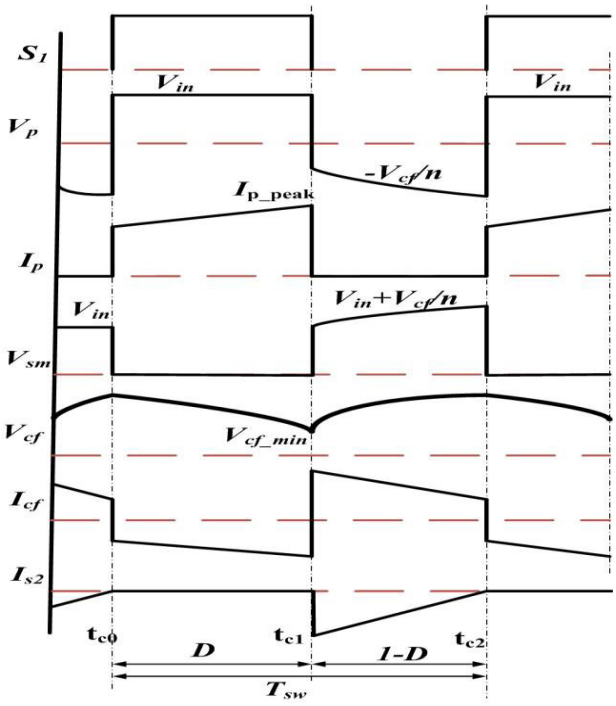

Fig 7:Steady-state operating waveforms of the for proposed inverter in CCM mode of operation

$$I_{s2}(t_{s1}) = -\frac{I_{p-peak}}{n} = -\frac{I_p(t_{s2}) + \left(\frac{V_{in}}{L_m} + \frac{n^2 V_{in}}{L_o}\right)(DT_s)}{n} \quad (24)$$

Output voltage of $-V_o$ is applied across the inductor L_o and the inductor current decreases linearly given by

$$i_{Lo}(t) = I_{Lo-peak} - \frac{V_o}{L_o}(t - DT_s) \quad (25)$$

Flying capacitor voltage V_{cf} appears across the magnetizing inductance, but the average voltage across the output capacitor and the flying capacitor is equal for given switching cycle ($<V_{cf}> = <V_o>$). Thus, for higher values of flying capacitance, V_{cf} is approximately equal to the output voltage V_o thus the current in flying capacitor I_{cf} increases linearly with a slope $V_o/(n^2 L_m)$ thus expression for switch current can be given as

$$I_{s2}(t_{c1}) = -\frac{I_{p-peak}}{n} + \frac{V_o}{L_o}(t - t_{c1}) + \frac{V_o}{n^2 L_m}(t - t_{c1}) \quad (26)$$

For CCM operation, switch S_m is turned-on before the diode current reaches zero. Thus, the currents at the end of this interval are equal to currents at the start of next interval.

$$I_p(t = t_{c0}) = -n\left(I_{s2}(T_s)\right) \quad (27)$$

$$I_{Lm}(t = t_{c0}) = n\left(I_{cf}(T_s)\right) \quad (28)$$

Substituting (eqn.26) in (eqn.27) the expression for the initial current when the primary switch is turned-on can be obtained as

ISSN (ONLINE): 2454-9762
ISSN (PRINT): 2454-9762
Available online at www.ijarmate.com

International Journal of Advanced Research in Management, Architecture, Technology and Engineering (IJARMATE)
Vol. 3, Special Issue10, March 2017

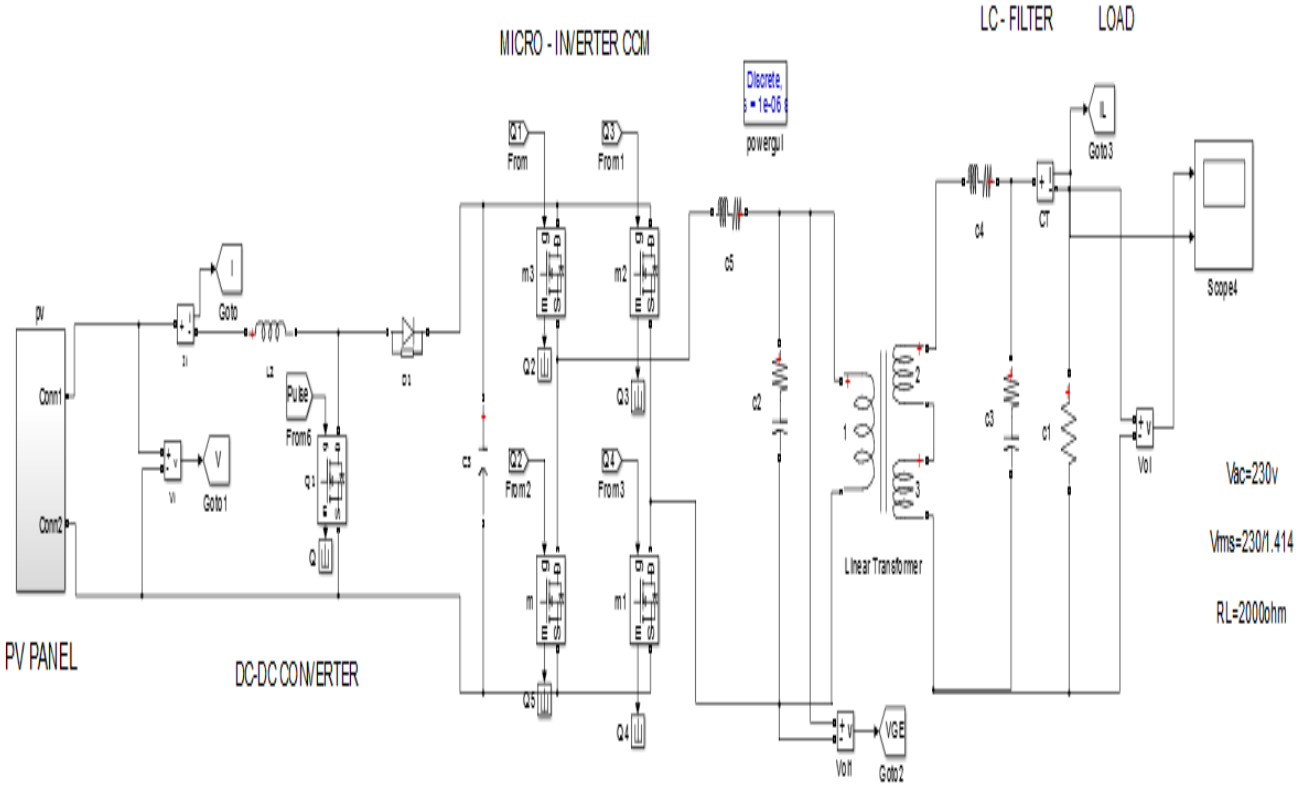

Fig 8:Simulation setup of Single Stage CCM Zeta Micro Inverter

$$I_o(t_{cD}) = n\left(\frac{I_{p-p+r}}{n} - (1 - DT_s)\left(\frac{V_g}{L_o} + \frac{V_g}{n^2 L_m}\right)\right) \quad (29)$$

From the above analysis, it should be realized that CCM operation of zeta micro-inverter results into lower RMS to average current ratio compared to DCM mode as the current ripple in the inductors L_m, L_o are reduced. This will in turn translate into improved inverter efficiency as the conduction losses are reduced.

IV RESULTS OF REAL-TIME VALIDATION

A solar micro-inverter, or simply micro inverter, is a device used in photovoltaics that converts direct current generated by a single solar module to alternating current. The output from several micro inverters is combined and often fed to the electrical grid. Micro inverters contrast with conventional string and central solar inverters, which are connected to multiple solar modules or panels of the PV system.

The proposed system was simulated in MATLAB/Simulink software. MATLAB (matrix laboratory) is a multiparadigm numerical computing environment and fourth-generation programming language. A proprietary programming language developed by MathWorks. MATLAB allows matrix manipulations, plotting of functions and data implementation of algorithms, creation of user interfaces and interfacing with programs written in other languages, including C, C++, Java, Fortran and Python. The converter was implemented with input voltage in the range 40-50V and the grid reference voltage was considered to be 110V. The main power switch, S_1 is operated at a high frequency of 60 kHz. The input to the converter is fed from a simulation model of PV system. MPPT technique employing fuzzy logic is implemented for efficient utilization of the PV array.

Microinverter at 20kHz theoretical loss distributions for zeta microinverter in CCM and DCM modes respectively, at different load conditions. It should be observed that at any load conditions the losses in CCM zeta microinverter are lower than DCM counterpart for the given specifications (low voltage high current input, high voltage boost ratio). This can be explained by considering RMS to average current ratio. At any value of given power transfer, RMS current through the components under DCM mode is be higher than CCM mode.

The Fig 8 shows the PV panel connected to the DC-DC converter. The PV panel output is DC. DC-DC converter tracks the maximum current. Then the DC-DC converter connected to the micro inverter. Micro inverter consists of four switches. If two switches are open, the other two switches are closed. If the arrangements are changed means not compare to the output. The output is analog pulse.

ISSN (ONLINE): 2454-9762
ISSN (PRINT): 2454-9762
Available online at www.ijarmate.com

International Journal of Advanced Research in Management, Architecture, Technology and Engineering (IJARMATE)
Vol. 3, Special Issue10, March 2017

Analog pulses are increase and decrease, so ac filter is used to reduce the losses.

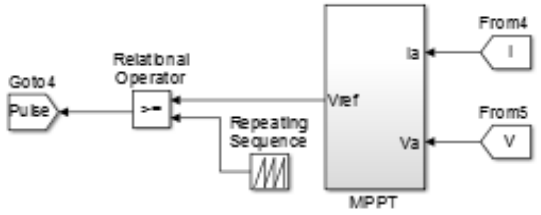

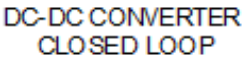

Fig 9:DC-DC Converter Closed loop

The Fig 9 represents the DC-DC converter loop is mounted on the PV panel. The MPPT is used to track the maximum DC Current. Then the closed loop of the DC-DC converter is used to check the output current with the reference current. The operating value of the system will be focused by the closed loop control.

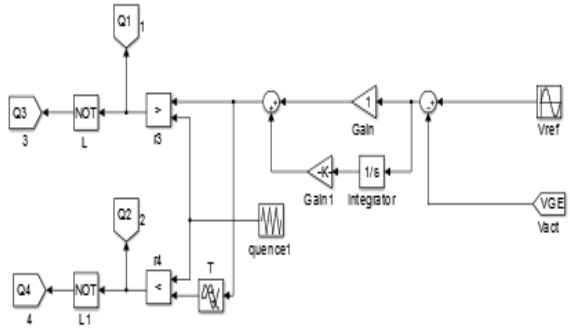

Fig 10:Micro inverter Close loop

From Fig 10, the micro inverter consists of four switches. The two switches are operate at a time. If the switches $S_1$and S_3 are closed then the switches $S_2$and S_4 are open.

The switching technique are available in the micro inverter. So the continuous turn ON and turn OFF process the constant current flows through the system. Then the micro inverter operate at continuous conduction mode. So the current stresses are reduced.

Table1:Simulation Parameters

S.No.	Parameter(unit)	Specification
1.	Input Voltage (V)	50
2.	Grid Reference Voltage (V)	110
3.	Frequency (kHz)	60
4.	Micro inverter frequency (kHz)	20

Table 1 shows the simulation parameters that is used to setup the Single Stage CCM Zeta Micro Inverter.

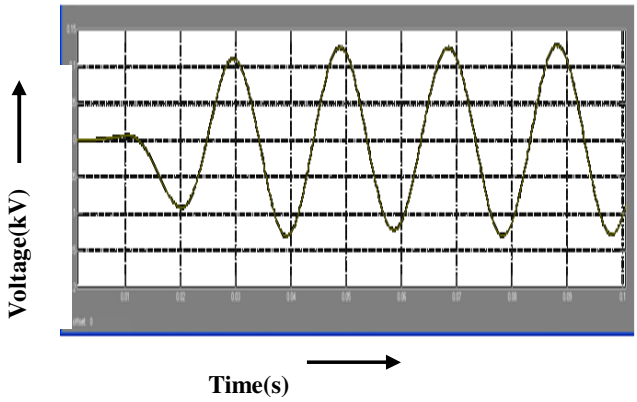

Fig 11: CCM Zeta eform

Fig 11 shows the voltage waveform of CCM Zeta microinverter. The graph is drawn between the voltage of the time. The voltage of the CCM Zeta microinverter is taken in the Y axis the time interval is taken in X axis. The steady state voltage obtained from CCM Zeta microinverter is about 230kV.

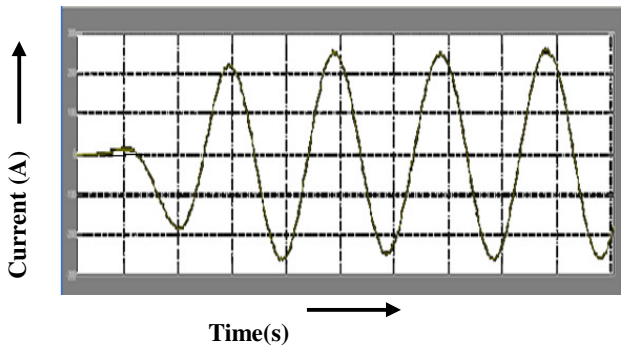

ISSN (ONLINE): 2454-9762
ISSN (PRINT): 2454-9762
Available online at www.ijarmate.com

International Journal of Advanced Research in Management, Architecture, Technology and Engineering (IJARMATE)
Vol. 3, Special Issue10, March 2017

Fig.4.4 CCM Zeta Micro inverter Current Waveform

Fig.4.5 shows the current waveform of CCM Zeta microinverter. The graph is drawn between the current of the time. The current of the CCM Zeta microinverter is taken in the Y axis the time interval is taken in X axis. The steady state current obtained from CCM Zeta microinverter is about 80A.

Table 4.2 Comparison of Voltage in MPPT and Zeta CCM Micro inverter

Time(s)	Voltage(kV)	
	MPPT	CCM Zeta Micro inverter
0.09	10	5
0.095	10	8
0.1	10	12
0.15	10	15
0.2	10	15

Table 4.2 shows the comparison between MPPT and CCM Micro-inverter. In CCM Micro-inverter strategy the voltage obtained is 10kV through the time period. But in CCM Micro-inverter strategy the voltage is increased as the time period increases.

Table 4.3 Comparison of Current in MPPT and Zeta CCM Micro inverter

Time(s)	Current(A)	
	MPPT	CCM Zeta Micro inverter
0.09	50	80
0.095	50	150
0.1	80	230
0.15	80	230
0.2	80	230

Table 4.3 shows the comparison between MPPT and CCM Zeta Micro-inverter. In CCM Zeta Micro-inverter strategy the current obtained is 80A through the time period. But in CCM Zeta Micro-inverter strategy the current is increased as the time period increases.

V CONCLUSION

A single stage CCM zeta micro inverter has been proposed for solar PVAC module. Steady-state operation and analysis of proposed zeta micro inverter in both DCM and CCM has been studied. Micro inverter operation in CCM mode results in reduced conduction losses, switch ratings and current stress. The proposed inverter provides HF isolation and has only a single switch operating at HF which will reduce the switching losses. The circuit is simple and easy to develop. Critical factors to consider while designing the inverter have been discussed and studied. A 220 W inverter prototype has been developed and tested in the laboratory to validate the claims, proposed operation and design. The laboratory prototype has a peak efficiency of 93% at rated power of 220 W.

REFERENCES

[1] Carrasco J. M ., Franquelo L. G., J. T. Bialasiewicz J. T., Galvan E., Guisado R. C. P., Prats M. A. M., Leon J. I. and Alfonso N.M.(2006) 'Power-electronic systems for the grid integration of renewable energy sources: A survey' IEEE Trans. Ind. Electron, vol. 53, no. 4, pp. 1002–1016.

[2] ChoiW.Y. (2013) 'High-Efficiency DC-DC Converter With Fast Dynamic Response for Low-Voltage Photovoltaic Sources', IEEE Trans. Power Electron, vol. 28, no. 2, pp. 706-716.

[3] Fongang EdwinF., Xiao W. andKhadkikarV. (2014) 'Dynamic modeling and control of interleaved flyback module-integrated converter for PV power applications', IEEE Trans. Ind. Electron, vol. 61, no. 3, pp. 1377-1388.

[4] Guisado P., Prats M. A. M., Leon J. I. and Alfonso N.M. (2006) 'Power-electronic systems for the grid integration of renewable energy sources: A survey', IEEE Trans. Ind. Electron, vol. 53, no. 4, pp. 1002–1016.

[5] Haibing H., Harb S., Kutkut N.H., Shen Z.J. and Batarseh I. (2013) 'A single stage microinverter without using electrolytic capacitors', IEEE Trans. Power Electron, vol. 28, no. 5, pp. 2677-2687.

ISSN (ONLINE): 2454-9762
ISSN (PRINT): 2454-9762
Available online at www.ijarmate.com

International Journal of Advanced Research in Management, Architecture, Technology and Engineering (IJARMATE)
Vol. 3, Special Issue10, March 2017

[6] Haibing H., Harb S., Xiang F., Dehua Z., Qian Y., Shen Z.J. and Batarseh I. (2012) 'A three-port flyback for PV microinverter applications with power pulsation decoupling capability', IEEE Trans. Power Electron, vol. 27, no. 9, pp. 3953-3964.

[7] Jiang S., Cao D., Li Y. and Peng F. Z. (2012) 'Grid-Connected Boost-Half-Bridge Photovoltaic Microinverter System Using Repetitive Current Control and Maximum Power Point Tracking', IEEE Trans. Power Electron., vol. 27, no. 11, pp. 4711-4722.

[8] Kim Y.H., Ji Y.H., Kim J.G., Jung Y.C. and Won C.Y. (2013) 'A new control strategy for improving weighted efficiency in photovoltaic AC module-type interleaved flyback inverters', IEEE Trans. Power Electron, vol. 28, no. 6, pp. 2688-2699.

[9] Kjaer S.B., Pedersen J. K. and Blaabjerg F. (2005) 'A review of single-phase grid-connected inverters for photovoltaic modules', IEEE Trans. Ind. Appl, vol. 41, no. 5, pp. 1292-1306.

[10] Kyritsis C., Tatakis E.C. and Papanikolaou N.P. (2008) 'Optimum design of the current-source flyback inverter for decentralized grid-connected photovoltaic systems', IEEE Trans. Energy Convers, vol. 23, no. 1, pp. 281-293.

[11] Li Q. and Wolfs P. (2007) 'A current fed two-inductor boost converter with an integrated magnetic structure and passive lossless snubbers for photovoltaic module integrated converter applications', IEEE Trans. Power Electron, vol. 22, no. 1, pp. 309–321.

[12] Li Q. and Wolfs P. (2008) 'A review of the single phase photovoltaic module integrated converter topologies with three different DC link configurations', IEEE Trans. Power Electron, vol. 23, no. 3, pp. 1320-1333.

[13] Liu B., Duan S. and Cai T. (2011) 'Photovoltaic DC-building-module-based BIPV system Concept and design considerations', IEEE Trans. Power Electron, vol. 26, no. 5, pp. 1418-1429.

[14] Nayanasiri D. R., Vilathgamuwa D. M. and Maskell D. L. (2013) 'Half-Wave Cycloconverter Based Photovoltaic Microinverter Topology with Phase Shift Power Modulation', IEEE Trans. Power Electron, vol. 28, no. 6, pp. 2700-2710.

[15] Rodriguez C. and Amaratunga G. (2008) 'Long-lifetime power inverter for photovoltaic AC modules', IEEE Trans. Ind. Electron, vol. 55, no. 7, pp. 2593-260.

[16] Viero, R.C., Lopez, H.F.M., Zollmann, C.A., Reis, F.S. (2010) 'Dynamic modeling of a sinusoidal inverter based on ZETA converter working in DCM for PV arrays', in proc. 36th Annual Conference on IEEE Industrial Electronics Society(IECON), pp. 439-444.

[17] Vuthchhay E and Bunlaksananusorn, C., (2010) 'Modeling and Control of a Zeta Converter', in proc. Power electronics conference (IPEC), pp. 612-619.

[18] Yang B., Li W., Gu Y., Cui W. and He X. (2012) 'Improved transformerless inverter with common-mode leakage current elimination for a photovoltaic grid-connected power system', IEEE Trans. Power Electron, vol. 27, no. 2, pp. 752-762.

[19] Yanlin L. and Oruganti R. (2012) 'A low cost flyback CCM inverter for ac module applications', IEEE Trans. Power Electron, vol. 27, no. 3, pp. 1295-1303.

[20] Yao-Ching Hsieh, Ming-Ren Chen and Hung-Liang Cheng, (2011) 'An interleaved flyback converter featured with zero-voltage transition', IEEE Trans. Power Electron, vol. 26, pp. 79-84.

[21] Yu W., Lai J.-S., Qian H., Hutchens C., Zhang J. (2010) 'High-efficiency inverter with H6-type configuration for photovoltaic non-Isolated AC module applications', in Proc. of IEEE Applied Power Electronics Conference and Exposition(APEC), Palm Springs, CA, pp. 1056-1061.